Graphical abstract

Immobilization of sulfonated polysulfone via 2D LDH nanosheets during phase-inversion: A novel strategy towards greener membrane synthesis and enhanced desalination performance

Peng Lu[1,2], Yi Wang[3]*, Ling Wang[1,2], Yayu Wei[1,2], Wenjun Li[1,2], Yanshuo Li[1,2]*, Chuyang Y. Tang[4]*

[1]School of Materials Science and Chemical Engineering, Ningbo University, Ningbo, 315211, P. R. China

[2]State Key Laboratory Base of Novel Functional Materials and Preparation Science, School of Materials Science & Chemical Engineering, Ningbo University, Ningbo, 315211, P. R. China

[3]State Key Lab of NBC for Protect Civilian, Beijing, 102205, P. R. China

[4]Department of Civil Engineering, the University of Hong Kong, Pokfulam Road, 999077 Hong Kong, S.A.R., P. R. China

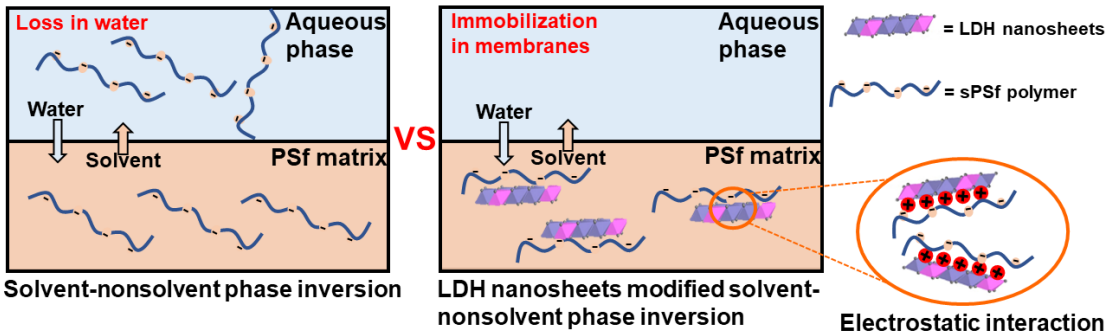

Immobilization of sulfonated polysulfone via 2D LDH nanosheets during phase-inversion: A novel strategy towards greener membrane synthesis and enhanced desalination performance

Peng Lu[1,2], Yi Wang[3]*, Ling Wang[1,2], Yayu Wei[1,2], Wenjun Li[1,2], Yanshuo Li[1,2]*, Chuyang Y. Tang[4]*

[1]School of Materials Science and Chemical Engineering, Ningbo University, Ningbo, 315211, P. R. China

[2]State Key Laboratory Base of Novel Functional Materials and Preparation Science, School of Materials Science & Chemical Engineering, Ningbo University, Ningbo, 315211, P. R. China

[3]State Key Lab of NBC for Protect Civilian, Beijing, 102205, P. R. China

[4]Department of Civil Engineering, the University of Hong Kong, Pokfulam Road, 999077 Hong Kong, S.A.R., P. R. China

*Corresponding author:

Prof. Yanshuo Li,

School of Materials Science and Chemical Engineering, Ningbo University, 818 Fenghua Road, Ningbo, 315211, P. R. China

State Key Laboratory Base of Novel Functional Materials and Preparation Science, School of Materials Science & Chemical Engineering, Ningbo University, Ningbo, 315211, P. R. China

E-mail: liyanshuo@nbu.edu.cn

Dr. Yi Wang,

State Key Lab of NBC for Protect Civilian, Beijing, 102205, P. R. China

E-mail: wangyi102205@sina.com

Prof. Chuyang Y. Tang,

Department of Civil Engineering, the University of Hong Kong, Pokfulam Road, 999077 Hong Kong, S.A.R., P. R. China

E-mail: tangc@hku.hk

Abstract

Sulfonated polysulfone (sPSf) is a commonly used hydrophilic additive to polysulfone (PSf) substrates for preparing polyamide membranes with enhancement desalination performance. However, severe leaching of water-soluble sPSf into the coagulation water bath during substrate formation can lead to weakened mechanical strength of the substrate, loss of the expensive sPSf polymer, and potential environmental pollution. In this study, we report a novel and efficient strategy to "anchor" sPSf in the PSf matrix by using 2D layered double hydroxide (LDH) nanosheets. LDH nanosheets effectively immobilized sPSf due to their electrostatic interaction, resulting in greener membrane synthesis. Substrates modified with LDH anchored sPSf ($PSf/sPSf_5$-LDH_x) exhibited enhanced mechanical strength and water permeability compared to the pristine PSf substrate as well as the sPSf-blended substrates ($sPSf/sPSf_5$). Interfacial polymerization on the $PSf/sPSf_5$-LDH_x substrate resulted in a polyamide rejection film containing more extensive nanovoids and thus greater effective filtration area, which enhanced water permeability without major loss of salt rejection. In forward osmosis tests, this novel membrane enjoyed an additional advantage of less severe internal concentration polarization, as reflected by its significantly reduced structural parameter.

1. Introduction

The global challenge of water scarcity [1] drives the exploitation of alternative water resources through membrane-based desalination and water reuse [2, 3]. Thin-film composite (TFC) membranes, with an ultrathin polyamide (PA) selective layer interfacially polymerized on top of a porous substrate [4, 5], are the most widely used commercial desalting membranes for nanofiltration, reverse osmosis (RO) and forward osmosis (FO) [6-9]. These membranes offer desired combinations of permeability and selectivity for a wide range of desalination and water reuse applications [10-12]. Nevertheless, further enhancing their permeability (for reduced energy consumption [13]) and selectivity (for improved water quality [11]) is challenging due to the strong trade–off between water permeability and selectivity, i.e., increasing water permeability generally leads to a reduction in salt rejection [14, 15].

Substrate properties play a critical role on membrane separation properties. For example, coating the porous substrate with a layer of tannic acid-Fe(III) [16] or carbon nanotubes [17] led to one order of magnitude enhancement in water permeability of the resulting TFC membranes. Incorporating hydrophilic polymers for substrate preparation is another effective strategy, with several studies reported improved membrane permselectivity [18-20] and stronger binding between the PA layer and the substrate [21, 22]. For FO membranes, the use of hydrophilic substrates offers an additional advantage by reducing their internal concentration polarization (ICP) [23]. One commonly used hydrophilic additive is sulfonated polysulfone (sPSf), with its polymeric backbone structurally similar to polysulfone (PSf) and its sulfonate

functional groups imparting hydrophilicity [24, 25]. A recent study reported improved water flux and lower reverse salt flux for an FO membrane with sPSf blended in its porous substrate [26]. Nevertheless, severe leaching of water-soluble sPSf into the coagulation water bath during substrate formation can result in serious consequences, such as (1) weakened mechanical strength of the substrate (due to plasticization in the presence of water) [26]; (2) loss of expensive sPSf polymer [27]; and (3) environmental risks associated with the discharge of coagulation bath water.

This study reports a novel strategy of "anchoring" sPSf in a PSf substrate by layered double hydroxide (LDH) nanosheets incorporated via a modified solvent-nonsolvent phase inversion process (Figure 1). We hypothesize that the LDH nanosheets can immobilize sPSf in the PSf matrix due to their high affinity. The effects of LDH nanosheets on the properties of the substrate and the desalination performance of the resulting TFC membranes were systematically investigated. Our study provides an efficient and green strategy for mitigating sPSf leaching and simultaneously improving the mechanical properties and separation performance of TFC membranes.

2. Materials and methods

2.1 Materials and Chemicals.

Polysulfone (PSf, average Mn ~22,000 Da) was purchased from Sigma-Aldrich. Sulfonated polysulfone (sPSf) with 30% degree of sulfonation was purchased from Yanjin Technology Co., Ltd. The chemical structure of PSf and sPSf polymers as shown in Fig. S1. A commercial polyester nonwoven fabric (PET, grade 3249) was purchased from Ahlstrom. 1,3-phenylenedia-mine (MPD, >99%) and 1,3,5-benzenetricarbonyl

trichloride (TMC, ~98%) were purchased from TCI Chemicals Ltd. $Mg(NO_3)_2•6H_2O$, $Al(NO_3)_3•9H_2O$, NaOH, NaCl, $NaNO_3$, $NaHSO_3$, NaClO (available chlorine 8–12%) and 1-methyl-2-pyrrolidinone (NMP, anhydrous, ~99.5%) were purchased from Sinopharm Chemical Reagent Co., Ltd. DI-water was produced using a Milli-Q ultrapure water purification system (Millipore, Billerica, MA).

2.2 Intercalation-assisted exfoliation of LDH nanosheets.

MgAl-NO_3 LDHs were prepared using a method modified from Wang and coworkers [28] (also see Figure S2 in the Supporting Information). Briefly, 9.62 g $Mg(NO_3)_2•6H_2O$ and 4.69 g $Al(NO_3)_3•9H_2O$ were added in 50 ml DI water (referred as solution A), and 2.12 g $NaNO_3$ was added in 50 ml DI water (referred as solution B). Before using, these solutions were sparged with N_2 gas to remove dissolved CO_2. Next, solution A was dropwise added to solution B while maintaining pH at 10 by the addition of 3.4 M NaOH solution. The mixture was aged for 1 h at room temperature under continuous stirring, then hydrothermally treated at 120 °C for 12 h. After hydrothermal aging, the resulting MgAl-NO_3 LDHs were washed with DI water until pH = 7 and further washed with acetone to prevent nanoparticles agglomeration [29]. The obtained MgAl-NO_3 LDHs were dried at 100 °C in an oven. A certain amount of MgAl-NO_3 LDHs was dispersed into an NMP solution under stirring. To facilitate the exfoliation, the dispersed solution was treated by a 30 min ultrasonication. The concentration of delaminated MgAl-NO_3 LDHs dispersions were adjusted to 1, 2, 4, and 6 g L^{-1}, respectively. To obtain LDH nanosheets for further material characterization, the delaminated LDH dispersions were centrifuged at 10,000 rpm for 10 min to extract

exfoliated LDH nanosheets.

2.3 Preparation of LDH nanosheets modified TFC membranes.

LDH nanosheets modified substrates were fabricated using the solvent-nonsolvent induced phase-inversion method. Table 1 shows the key parameters of casting solutions. Typically, 5 wt% (which based on the total mass of polymers) sPSf granules with 30% sulfonation degree was dissolved in a LDH-NMP dispersion solution (1, 2, 4, or 6 g L^{-1}), and stirred at room temperature for 12 h. PSf granules were then dissolved in above solution and subjected to magnetic stirring for 12 h. The above casting dope was degassed for another 8 h before being casted on a wetted PET fabric with a 150 μm casting knife (Elcometer 3530). Finally, the casted substrates were immediately immersed in a DI water bath for at least 24 h. These LDH nanosheets modified substrates are named as PSf/$sPSf_5$-LDH_x, where the subscripts 5 indicates the wt% of sPSf and *x* indicates LDH concentration. For comparison purpose, additional PSf/sPSf substrates without LDH (denoted as PSf/$sPSf_5$, PSf/$sPSf_{10}$, and PSf/$sPSf_{15}$ in accordance to the wt% of sPSf) and PSf substrate were also prepared.

Polyamide (PA) rejection layer was formed on the as-prepared substrates by the IP reaction of MPD and TMC monomers following our previous works [30, 31]. The detailed preparation process is shown in Figure S2 of the Supporting Information. Finally, the prepared membranes were thoroughly rinsed with DI-water and stored in DI-water at 4 °C till later usage. The TFC PA membranes are denoted as PA@substrate (e.g., PA@PSf/$sPSf_5$-LDH_x stands for PA membranes prepared on PSf/$sPSf_5$-LDH_x substrates).

2.4 Characterization of LDH nanosheets.

The morphologies of samples were characterized by field-emission scanning electron microscope (SEM, Nova NanoSEM 450) and high-resolution transmission electron microscopy (HR–TEM, JEOL JEM–2100Plus), respectively. XRD characterization (D8 ADVANCE, Bruker) evaluated the delaminated degree of LDHs in NMP solution. Diffraction patterns were recorded with in the range of 2θ = 5–30° with a step size of 0.02°. The turbidity of the delaminated LDHs dispersions in NMP was measured using a turbidimeter (WGZ-200, Shanghai Shanke Instrument). The particle size and zeta potential of delaminated LDH dispersions were measured using particle size-zeta potential analyzer. (Nano–ZS, Malvern). Moreover, the zeta potential of 5 wt% sPSf–NMP solution was measured, which was used to evaluate the interaction mechanism.

2.5 Characterization of coagulation baths.

The leaching of water-soluble sPSf polymer during the phase-inversion was evaluated. Water samples were collected from the coagulation bath used for the phase-inversion, and their sPSf content was determined by a UV–Vis spectrophotometer (TU-1810, PERSEE). Residues of the coagulation baths were obtained by freeze-drying (FreeZone2.5, LABCONCO) at –50 °C for 48 h, then the functional groups were analyzed by an attenuated total reflectance flourier transform infrared spectroscopy (ATR-FTIR, VERTEX 70, Bruker).

2.6 Characterization of membranes.

Surface and cross-section of membranes were observed using SEM. The as-prepared membranes were carefully peel off the PET substrates, fractured in liquid nitrogen, and

coated with Pt using a sputtering coater before observations. The surface roughness and hydrophilicity of membranes were studied by atomic force microscope (AFM, Dimension 3100, Vecco) and contact angle system (DSA100, Krüss), respectively. The water uptake ratio was calculated from the weight gain of the membranes after sorption equilibrium in water as the ratio of this weight gain to the weight of the dry membranes. Mechanical properties of prepared substrates without commercial PET were characterized using a universal tensile tester (CMT4502, MTS) equipped with a 500 N load cell at a stretch speed of 10 mm min^{-1}. Before each measurement, a membrane sample was cut in a size of 20 mm×10 mm, and its thickness was measured with a digital micrometer.

2.7 Evaluation desalination performance of LDH modified TFC membranes.

Separation performance of the substrates and PA-based TFC membranes was evaluated by a cross-flow RO system (TYLG-19, Ji'nan Bona Biological Technology Co., Ltd) with an effective membrane surface area (A_m) of 15.90 cm^2. Pure water flux of substrates was measured at room temperature under 1 bar. The RO water flux of membranes was tested at room temperature under 3 bar of applied pressure (ΔP) after pre-compaction at 5 bar. Water flux J was calculated using equations (1):

$$J = \frac{\Delta V}{A_m \times \Delta t} \quad (1)$$

where ΔV and Δt are the permeate volume change and time interval, respectively. By using a 10 mM NaCl solution as feed solution, the NaCl rejection (R) of TFC membranes was determined by equation (2):

$$R = \left(1 - \frac{C_p}{C_f}\right) \times 100 \quad (2)$$

where C_p and C_f are the NaCl concentrations in the feed and permeation, respectively. The water permeability coefficient (A) and salt permeability coefficient (B) were calculated from equations (3) and (4) based on the solution-diffusion model[29, 32]:

$$A = J / (\Delta P - \Delta\pi) \quad (3)$$

$$B = (1 - R) / R * J \quad (4)$$

where $\Delta\pi$ is the osmotic pressure across the membrane.

FO performance of the TFC membranes was evaluated using a lab-scale cross-flow FO filtration unit with an effective membrane area (A_m) of 30.75 cm^2 following a standard methodology reported in the literature [33]. Membranes were tested under PRO mode (PA layer facing DS) and FO mode (PA layer facing FS), respectively. Each test was conducted for a duration of 1 h in triplicates. The water flux (J_w) and reverse salt flux (J_s) were calculated according to:

$$J_w = \frac{\Delta V}{A_m \Delta t} \quad (5)$$

$$J_s = \frac{\Delta C_t V_t}{A_m \Delta t} \quad (6)$$

where ΔV is the volume change of draw solution (DS) over a predetermined time Δt, C_t and V_t are the NaCl concentration change and volume of feed solution (FS) at the end of tests, respectively. The structural parameter (S) of membrane, an intrinsic property governing ICP effect in the substrate [32], is determined by fitting A and B values into equation (7) for the FO mode:

$$S = \frac{D}{J_w}\left[\ln\frac{A\pi_{draw} + B}{A\pi_{feed} + B + J_w}\right] \quad (7)$$

where π_{draw} and π_{feed} are the osmotic pressure of DS and FS, respectively. And D is the NaCl diffusion coefficient.

2.8 Trade-off and upper bound behavior of desalination membranes.

The trade-off relation between water permeability and water/salt selectivity according to the solution-diffusion mechanism, which could serve as a standard reference in the field of desalination membranes [14, 34-38]. Here, a preferred way is to plot the water/NaCl permselectivity A/B vs. the water permeance A. Figure 6b shows a clear tradeoff behavior, with the upper bound line given by:

$$\frac{A}{B} = 16000A^{-3.2} \quad \text{(with } A/B \text{ in bar}^{-1} \text{ and } A \text{ in L m}^{-2}\text{ h}^{-1}\text{ bar}^{-1}\text{)} \quad (8)$$

where A and B are obtained via the equations (3) and (4), respectively

3. Results and discussion

3.1 Exfoliation of LDH nanosheets.

Microscopic characterization of delaminated LDHs show plate-like nanosheets (Figure 2(a)) with a lateral size on the order of 100 nm (Figure 2(b)). XRD spectrum (Figure 2(c)) of the MgAl-NO_3 LDH powders show the characteristic 003 and 006 diffraction peaks indexed according to MgAl hydrotalcite (JCPDS No. 35-0965), confirming the well-developed layered structure [39]. After delamination, the 003 diffraction peak was greatly weakened and the 006 diffraction peak almost disappeared. Furthermore, a clear Tyndall light scattering was observed for LDH dispersed in NMP with low concentrations of 1–4 g L^{-1} (Figure S3(b)). These results confirm the successful

exfoliation of LDH nanosheets. However, higher LDH concentration (e.g., 6 g L^{-1}) led to incomplete delamination, as indicated by (1) the increased intensity of the 003 diffraction peak (Figure 2(c)), (2) the less obvious Tyndall light scattering (Figure S3(b)), and (3) the wider range of particle size distribution (Figure 2(d)).

3.2 Immobilization of sPSf during phase-inversion.

Leaching of sPSf during phase inversion was investigated by analyzing coagulation bath water used for various substrates. For PSf and the PSf/sPSf series, loading greater amount of sPSf resulted in greater turbidity (Figure 3a) and more intense UV absorption over 260-280 nm reflecting the presence of sulfonic groups [27] (Figure 3b). These results confirm that the hydrophilic sPSf can easily leach into the coagulation bath during the solvent-nonsolvent induced phase-inversion [40]. Introducing LDH nanosheets into the substrate significantly decreased the turbidity of coagulation baths (e.g., from 9.4 NTU for PSf/sPSf$_5$ to 1.5 NTU for PSf/sPSf$_5$-LDH$_6$, see Figure 3(a)), implying greatly reduced leaching of sPSf. Consistently, the UV–Vis spectra (Figure 3(b)) also show the diminishing of the absorption band over 260–280 nm.

Furthermore, ATR-FTIR characterization was performed for the residues of freeze-dried coagulation bath water (Figure 3(c)). The residues obtained from the PSf/sPSf$_x$ series show a characteristic peak at ~1030 cm^{-1} (assigned to the stretching vibrations of the S=O bond in sulfonic acid ($-SO_3^-$) groups [25]) whose intensity increased at greater sPSf loading. In contrast, this characteristic peak of sPSf gradually disappeared with increased LDH incorporation for the PSf/sPSf$_5$-LDH$_x$ series, accompanied with a greater presence of NO_3^- groups (peak at 1384 cm^{-1}) from the exfoliated LDH

nanosheets [41]. These ATR-FTIR results of the bath water residues are consistent with the turbidity and UV-VIS analysis, which underpins the role of LDH nanosheets in immobilization of sPSf in the PSf matrix. Additional ATR-FTIR characterization was also performed for the substrates (Figure S4). The SO_3^- peak (~1030 cm^{-1}) was present for the PSf/sPSf$_5$-LDH$_6$ substrate while it was much weaker for the PSf/sPSf$_5$ substrate, providing additional evidence that sPSf was effectively immobilized in the PSf matrix by the LDH nanosheets.

The strong affinity between LDH nanosheets and sPSf is ascribed to their opposite charges (Figure S5). The electrostatic interaction between positively charged LDH nanosheets and negatively charged sPSf allows sPSf to be anchored in the casted substrate (Figure 1) [28]. This simple anchoring strategy not only effectively prevents the loss of expensive sPSf polymer but also mitigates the environmental impact caused by the leaching of sPSf.

3.3 Effect of LDH nanosheets on properties of sPSf modified substrates.

Mechanical strength plays an important role in membrane separation, such as operation cycle and lifespan of the membranes [42]. Figure 4(a) shows mechanical stress-strain curves of the PSf, PSf/sPSf$_x$, and PSf/sPSf$_5$-LDH$_x$ substrates, respectively. Compare with the PSf substrate, introducing sPSf into the substrates (i.e., the PSf/sPSf$_x$ substrates) significantly weakened the mechanical properties. It can be attributed to the strongly polar -SO_3^- groups that increase polymer chain movements and thus make the substrates more flexible [43]. This undesirable effect can be addressed by the introduction of exfoliated LDH nanosheets into the substrate, with the PSf/sPSf$_5$-LDH$_x$

series showing much improved mechanical properties compared to both the PSf substrate and the PSf/sPSf$_x$ substrates. The stress improvement could be explained by the interactions established between LDH nanosheets and sPSf polymer chains. And the strain improvement could be attributed to a possible rearrangement of LDH nanosheets in the direction of the deformation, allowing higher membrane deformation [30, 44].

Hydrophilicity of the substrates was characterized by water contact angle measurements (Figure 4(b)). Both PSf/sPSf$_5$ and PSf/sPSf$_5$-LDH$_x$ had smaller contact angles compared to that of the PSf substrate, which is largely due to the introduction of hydrophilic sPSf into the substrates (Figure S6) [42]. Consistently, these substrates also had higher water uptake ratio. Introducing sPSf into the substrates resulted in reduced surface roughness (Figure S7), possibly due to a reduction of the solvent exchange rate between solvent and non-solvent by the hydrophilic polymer. Furthermore, it was found that the surface roughness of PSf/sPSf$_5$-LDH$_x$ substrates were further significantly decreased compared to PSf/sPSf$_5$ and PSf/sPSf$_5$-LDH$_x$. This may be explained by the increased viscosity of the casting solution due to the introduction of LDH nanosheets, which retards the exchange of solvent and non-solvent during phase-inversion [45-47]. In addition, the more positive surface charge of PSf/sPSf$_5$-LDH$_6$ substrate (Figure 4(c)) was obtained compared to the PSf/sPSf$_5$ and PSf/sPSf$_{15}$.

Water permeability of the substrate was also improved by introducing sPSf into the substrate (e.g., 146.3 L m^{-2} h^{-1} bar^{-1} for PSf/sPSf$_5$ vs. 96.7 L m^{-2} h^{-1} bar^{-1} for PSf, see Figure 4(d), thanks to the enhanced hydrophilicity (Figure 4(b)) and the more porous

structure (Figure 5(b)). After the introduction of LDH nanosheets, the PSf/sPSf$_5$-LDH$_4$ substrate displayed the highest water permeability of 212.8 L m^{-2} h^{-1} bar^{-1}, which was nearly 50% higher compared to the corresponding PSf/sPSf$_5$ substrate without LDH nanosheets. The water permeability of PSf/sPSf$_5$-LDH$_4$ was comparable to that of the PSf/sPSf$_{15}$ substrate (with 15% sPSf loading, see Figure S9). This result confirms that the effective anchoring of sPSf by LDH nanosheets could allow significant saving in sPSf consumption, e.g., from 15% to 5% in order to achieve the same effect on the substrate water permeability.

3.4 Effect of LDH nanosheets on the morphology of membranes.

The morphology of the substrates was investigated using SEM as shown in Figure 5(a-c). All the as-prepared substrates showed an asymmetric structure, consisting of a thin top layer and a porous bottom layer with finger-like macrovoids. Moreover, the PSf/sPSf$_5$ and PSf/sPSf$_5$-LDH$_4$ substrates showed more porous structures, which might be due to the improved hydrophilicity that induced a delayed demixing during the phase-inversion. However, the surface porosity of the sPSf blended substrates (e.g., PSf/sPSf$_5$ and PSf/sPSf$_{15}$ (Figure S10)) was decreased by ImageJ analysis. After IP reaction, all the resulting TFC membrane surfaces showed the characteristic "ridge-valley" morphology (Figure 5(d-f)) [48-51]. The cross-section of PA@PSf (Figure 5(d)) shows a PA layer with an apparent thickness of about 110 nm. It is worthwhile to note that, due to the presence of nanovoids in the PA layer [5, 51], the actual intrinsic thickness is much smaller (in the range of 10-20 nm [52]). PA@PSf/sPSf$_x$ had thicker apparent thicknesses (approximately 120 nm for PA@PSf/sPSf$_5$ (Figure 5(e)) and 160

nm for PA@PSf/sPSf$_{15}$ (Figure S10(b)), which is possibly caused by their more porous substrates [29, 32, 53]. Furthermore, the PA layer of PA@PSf/sPSf$_5$-LDH$_4$ had the greatest apparent thickness of approximately 230 nm, with much more extensive nanovoids contained inside this rejection layer (Figure 5(f)). According to our previous works [5, 51, 54, 55], nanovoids inside the PA layers are formed as a result of degassing of CO_2 nanobubbles during the IP reaction (i.e., the conversion of HCO_3^- dissolved in the MPD solution to CO_2 due to acid and heat generation during IP), and larger nanovoids are well correlated to improved membrane water permeability. Consistent with its larger nanovoids, PA@PSf/sPSf$_5$-LDH$_4$ also had a much larger surface roughness (R_a = 176 nm) compared to those of PA@PSf and PA@PSf/sPSf$_5$ (approximately 100 nm, see Figure S11). The greater roughness and more extensive nanovoids in the PA layer are favorable in increasing the effective filtration area (and thus membrane permeability [5, 52]).

3.5 Influence of LDH nanosheets on desalination performance.

The water permeability and NaCl rejection of the TFC membranes were measured by cross-flow RO tests (Figure 6). The PA@PSf/sPSf$_5$ membrane had a slightly higher water permeability of 3.15 L m^{-2} h^{-1} bar^{-1} compared to that of PA@PSf (2.92 L m^{-2} h^{-1} bar^{-1}, also see Table S1). The LDH nanosheets-incorporated PA@PSf/sPSf$_5$-LDH$_x$ membranes showed more effective enhancement, with the optimized membrane PA@PSf/sSPf$_5$-LDH$_4$ having a water permeability of 4.04 L m^{-2} h^{-1} bar^{-1}. This significantly enhanced membrane permeability compared to the control PA@PSf can be ascribed to the improved hydrophilicity and water permeability of the substrate

(Figure 4) as well as the formation of rougher PA layer with enhanced effective filtration area (Figure 5). Nevertheless, the loading of sPSf and LDH nanosheets led to a slight reduction in NaCl rejection (Figure 6(a) and Table S1). Figure 6(b) presents the trade-off between membrane water permeance (*A*) vs. the water/NaCl permselectivity (*A/B*) [14, 15, 38]. In general, the PA@PSf/sPSf$_5$-LDH$_x$ membranes overperformed the control PA@PSf membrane and the PA@PSf/sPSf$_x$ series, confirming sPSf immobilization by LDH as an effective strategy for tailoring membrane separation performance.

Additional FO tests were also performed using a 1 M NaCl draw solution (Figure 7). Consistent with the RO results, the PA@PSf/sPSf$_5$-LDH$_4$ membrane had the highest water flux in both FO and PRO modes. The combined effect of a more hydrophilic substrate and greater porosity led to a significant reduction in the structural parameter (Table S1) and therefore less severe ICP [30], which partially explains the water flux enhancement. In addition, the greater water permeability coefficient, resulting from the rougher PA layers with more extensive nanovoids [5, 51, 52], also contributes to more effective transport of water [30, 59]. In addition, the stability of the LDH nanosheets in the membranes was assessed by the PA@PSf/sPSf$_5$-LDH$_4$ membrane in the cross–flow filtration system at FO mode for 50 h. The concentration of Mg in the feed solution were detected by Atomic absorption spectrophotometer (AA-6880, SHIMADZU) analysis and the result is shown in Figure S12. The tested membrane contains approximately 10 mg LDH nanosheets. During the initial 6 h, the Mg release was not observed. The average release rate was about 0.04 ppm/12 h. Unlike some other

nanomaterials that releases toxic heavy metals (e.g., Ag, Cu, etc.), Mg is present in natural water in abundance and does not harm human health.

4. Conclusions

The current study presents a novel and green strategy for immobilizing sPSf in the substrates, which effectively anchors sPSf in the substrates via electrostatic interaction and prevents its leaching to the coagulation bath during the phase-inversion process. And the method of exfoliated LDH nanosheets can effectively improved the properties of PSf/sPSf$_5$ membrane, which achieved the similar performance under the higher sPSf loading (e.g., the PSf/sPSf$_{15}$). The resulting PSf/sSPf$_5$-LDH$_x$ substrates had higher mechanical strength, hydrophilicity and water permeability compared to the pristine PSf substrate. Compared to the control TFC@PSf membrane, the LDH-loaded TFC membranes showed enhanced water permeability, better combinations of permeability/selectivity (closer to the “upper bound"), and reduced structural parameters, leading to improved RO and FO performances. This novel approach shed new lights on the integration of advanced nanomaterials into the membrane preparation process for simultaneously enhanced desalination performance and reduced environmental impact.

Acknowledgments

This work is financially supported by the National Natural Science Foundation of China (21761132009), the Zhejiang Provincal Natural Science Foundation (LQ19E080005, LR18B060002), the Ningbo Natural Science Foundation (2019A610140), S&T

Innovation 2025 Major Special Programme (No: 2018B10018) and sponsored by K.C. Wong Magna Fund in Ningbo University.

References

[1] M.A. Montgomery, M. Elimelech, Water and sanitation in developing countries: including health in the equation, Environ. Sci. Technol., 41 (2007) 17-24.

[2] M. Elimelech, W.A. Phillip, The future of seawater desalination: energy, technology, and the environment, Science, 333 (2011) 712-717.

[3] C.Y. Tang, Z. Yang, H. Guo, J.J. Wen, L.D. Nghiem, E. Cornelissen, Potable water reuse through advanced membrane technology, Environ. Sci. Technol., 52 (2018) 10215-10223.

[4] Z. Tan, S. Chen, X. Peng, L. Zhang, C. Gao, Polyamide membranes with nanoscale Turing structures for water purification, Science, 360 (2018) 518-521.

[5] X. Song, B. Gan, S. Qi, H. Guo, C.Y. Tang, Y. Zhou, C. Gao, Intrinsic nanoscale structure of thin film composite polyamide membranes: Connectivity, defects, and structure-property correlation, Environ. Sci. Technol., 54 (2020) 3559-3569.

[6] J. Ren, J.R. McCutcheon, A new commercial thin film composite membrane for forward osmosis, Desalination, 343 (2014) 187-193.

[7] G. Amy, N. Ghaffour, Z. Li, L. Francis, R.V. Linares, T. Missimer, S. Lattemann, Membrane-based seawater desalination: Present and future prospects, Desalination, 401 (2017) 16-21.

[8] J.M. Gohil, P. Ray, A review on semi-aromatic polyamide TFC membranes prepared by interfacial polymerization: Potential for water treatment and desalination, Sep. Purif. Technol., 181 (2017) 159-182.

[9] C. Y. Tang, Y. N. Kwona, J.O. Leckiea, Effect of membrane chemistry and coating layer on physiochemical properties of thin film composite polyamide RO and NF membranes I. FTIR and XPS characterization of polyamide and coating layer chemistry, Desalination, 242 (2009) 149–167.

[10] N.T. Hancock, P. Xu, D.M. Heil, C. Bellona, T.Y. Cath, Comprehensive bench- and pilot-scale investigation of trace organic compounds rejection by forward osmosis, Environ. Sci. Technol., 45 (2011) 8483-8490.

[11] J.R. Werber, A. Deshmukh, M. Elimelech, The critical need for increased

selectivity, not increased water permeability, for desalination membranes, Environ. Sci. Technol. Lett., 3 (2016) 112-120.

[12] C. Y. Tang, Y. N. Kwona, J.O. Leckiea, Effect of membrane chemistry and coating layer on physiochemical properties of thin film composite polyamide RO and NF membranes II. Membrane physiochemical properties and their dependence on polyamide and coating layers, Desalination, 242 (2009) 168–182.

[13] D. Cohen-Tanugi, R.K. McGovern, S.H. Dave, J.H. Lienhard, J.C. Grossman, Quantifying the potential of ultra-permeable membranes for water desalination, Energ. Environ. Sci., 7 (2014) 1134-1141.

[14] Z. Yang, H. Guo, C.Y. Tang, The upper bound of thin-film composite (TFC) polyamide membranes for desalination, J. Membr. Sci., 590 (2019) 117297.

[15] J.R. Werber, C.O. Osuji, M. Elimelech, Materials for next-generation desalination and water purification membranes, Nat. Rev. Mater., 1 (2016) 16018.

[16] Z. Yang, Z.W. Zhou, H. Guo, Z. Yao, X.H. Ma, X. Song, S.P. Feng, C.Y. Tang, Tannic acid/Fe(3+) nanoscaffold for interfacial polymerization: Toward enhanced nanofiltration performance, Environ. Sci. Technol., 52 (2018) 9341-9349.

[17] Z. Zhou, Y. Hu, C. Boo, Z. Liu, J. Li, L. Deng, X. An, High-performance thin-film composite membrane with an ultrathin spray-coated carbon nanotube interlayer, Environ. Sci. Technol. Lett., 5 (2018) 243-248.

[18] Y. Yin, J. Fang, Y. Cui, K. Tanaka, H. Kita, K.-i. Okamoto, Synthesis, proton conductivity and methanol permeability of a novel sulfonated polyimide from 3-(2′,4′-diaminophenoxy)propane sulfonic acid, Polymer, 44 (2003) 4509-4518.

[19] W.R. Bowen, T.A. Doneva, H.B. Yin, Polysulfone-sulfonated poly(ether ether) ketone blend membranes: systematic synthesis and characterisation, J. Membr. Sci., 181 (2001) 253-263.

[20] N. Widjojo, T.-S. Chung, M. Weber, C. Maletzko, V. Warzelhan, A sulfonated polyphenylenesulfone (sPPSU) as the supporting substrate in thin film composite (TFC) membranes with enhanced performance for forward osmosis (FO), Chem. Eng. J., 220 (2013) 15-23.

[21] K.Y. Wang, T.-S. Chung, G. Amy, Developing thin-film-composite forward osmosis membranes on the PES/SPSf substrate through interfacial polymerization, AIChE J., 58 (2012) 770-781.

[22] Z. Yao, H. Guo, Z. Yang, C. Lin, B. Zhu, Y. Dong, C.Y. Tang, Reactable substrate participating interfacial polymerization for thin film composite membranes with enhanced salt rejection performance, Desalination, 436 (2018) 1-7.

[23] J.R. McCutcheon, M. Elimelech, Influence of membrane support layer hydrophobicity on water flux in osmotically driven membrane processes, J. Membr. Sci., 318 (2008) 458-466.

[24] H.-G. Yuan, Y.-Y. Liu, T.-Y. Liu, X.-L. Wang, Self-standing nanofilms of polysulfone doped with sulfonated polysulfone via solvent evaporation for forward osmosis, J. Membr. Sci., 523 (2017) 567-575.

[25] D. Grinic, M. Giagnorio, A. Cosola, F. Ricceri, M.C. Zanetti, M. Sangermano, A. Tiraferri, Maximizing the degree of sulfonation of polysulfone supports in TFC membranes for osmotically driven processes, Macromol. Mater. Eng., 303 (2018) 1800384.

[26] J. Ren, B. O'Grady, G. deJesus, J.R. McCutcheon, Sulfonated polysulfone supported high performance thin film composite membranes for forward osmosis, Polymer, 103 (2016) 486-497.

[27] J.F. Blanco, Q.T. Nguyen, P. Schaetzel, Novel hydrophilic membrane materials: sulfonated polyethersulfone Cardo, J. Membr. Sci., 186 (2001) 267-279.

[28] J. Wang, X. Mei, L. Huang, Q. Zheng, Y. Qiao, K. Zang, S. Mao, R. Yang, Z. Zhang, Y. Gao, Z. Guo, Z. Huang, Q. Wang, Synthesis of layered double hydroxides/graphene oxide nanocomposite as a novel high-temperature CO_2 adsorbent, J. Energ. Chem., 24 (2015) 127-137.

[29] P. Lu, W.J. Li, S. Yang, Y.Y. Wei, Z.G. Zhang, Y.S. Li, Layered double hydroxides (LDHs) as novel macropore-templates: The importance of porous structures for forward osmosis desalination, J. Membr. Sci., 585 (2019) 175-183.

[30] P. Lu, S. Liang, L. Qiu, Y. Gao, Q. Wang, Thin film nanocomposite forward

osmosis membranes based on layered double hydroxide nanoparticles blended substrates, J. Membr. Sci., 504 (2016) 196-205.

[31] P. Lu, W. Li, S. Yang, Y. Liu, Q. Wang, Y. Li, Layered double hydroxide-modified thin–film composite membranes with remarkably enhanced chlorine resistance and anti-fouling capacity, Sep. Purif. Technol., 220 (2019) 231-237.

[32] M. Rastgar, A. Bozorg, A. Shakeri, Novel dimensionally controlled nanopore forming template in forward osmosis membranes, Environ. Sci. Technol., 52 (2018) 2704-2716.

[33] T.Y. Cath, M. Elimelech, J.R. McCutcheon, R.L. McGinnis, A. Achilli, D. Anastasio, A.R. Brady, A.E. Childress, I.V. Farr, N.T. Hancock, J. Lampi, L.D. Nghiem, M. Xie, N.Y. Yip, Standard methodology for evaluating membrane performance in osmotically driven membrane processes, Desalination, 312 (2013) 31-38.

[34] M.R. Chowdhury, J. Steffes, B.D. Huey, J.R. McCutcheon, 3D printed polyamide membranes for desalination, Science, 361 (2018) 682-686.

[35] N.Y. Yip, M. Elimelech, Performance limiting effects in power generation from salinity gradients by pressure retarded osmosis, Environ. Sci. Technol., 45 (2011) 10273-10282.

[36] N.Y. Yip, A. Tiraferri, W.A. Phillip, J.D. Schiffman, L.A. Hoover, Y.C. Kim, M. Elimelech, Thin-film composite pressure retarded osmosis membranes for sustainable power generation from salinity gradients, Environ. Sci. Technol., 45 (2011) 4360-4369.

[37] C. Klaysom, T.Y. Cath, T. Depuydt, I.F. Vankelecom, Forward and pressure retarded osmosis: potential solutions for global challenges in energy and water supply, Chem. Soc. Rev., 42 (2013) 6959-6989.

[38] G.M. Geise, H.B. Park, A.C. Sagle, B.D. Freeman, J.E. McGrath, Water permeability and water/salt selectivity tradeoff in polymers for desalination, J. Membr. Sci., 369 (2011) 130-138.

[39] J. Wang, L. Huang, Y. Gao, R. Yang, Z. Zhang, Z. Guo, Q. Wang, A simple and reliable method for determining the delamination degree of nitrate and glycine intercalated LDHs in formamide, Chem. Commun. (Camb), 50 (2014) 10130-10132.

[40] Y. Wang, T. Xu, Anchoring hydrophilic polymer in substrate: An easy approach for improving the performance of TFC FO membrane, J. Membr. Sci., 476 (2015) 330-339.

[41] Y. Zhao, W. Yang, Y. Xue, X. Wang, T. Lin, Partial exfoliation of layered double hydroxides in DMSO: a route to transparent polymer nanocomposites, J. Mater. Chem., 21 (2011) 4869-4874.

[42] D. Song, J. Xu, Y. Fu, L. Xu, B. Shan, Polysulfone/sulfonated polysulfone alloy membranes with an improved performance in processing mariculture wastewater, Chem. Eng. J., 304 (2016) 882-889.

[43] B. Smitha, Synthesis and characterization of proton conducting polymer membranes for fuel cells, J. Membr. Sci., 225 (2003) 63-76.

[44] P. Anadão, L.F. Sato, H. Wiebeck, F.R. Valenzuela-Díaz, Montmorillonite as a component of polysulfone nanocomposite membranes, Appl. Clay Sci., 48 (2010) 127-132.

[45] M.J. Park, S. Phuntsho, T. He, G.M. Nisola, L.D. Tijing, X.-M. Li, G. Chen, W.-J. Chung, H.K. Shon, Graphene oxide incorporated polysulfone substrate for the fabrication of flat-sheet thin-film composite forward osmosis membranes, J. Membr. Sci., 493 (2015) 496-507.

[46] S. Qiu, L. Wu, X. Pan, L. Zhang, H. Chen, C. Gao, Preparation and properties of functionalized carbon nanotube/PSF blend ultrafiltration membranes, J. Membr. Sci., 342 (2009) 165-172.

[47] J.H. Choi, J. Jegal, W.N. Kim, Fabrication and characterization of multi-walled carbon nanotubes/polymer blend membranes, J. Membr. Sci., 284 (2006) 406-415.

[48] L. Shen, W.-s. Hung, J. Zuo, X. Zhang, J.-Y. Lai, Y. Wang, High-performance thin-film composite polyamide membranes developed with green ultrasound-assisted interfacial polymerization, J. Membr. Sci., 570-571 (2019) 112-119.

[49] X. Song, B. Gan, Z. Yang, C.Y. Tang, C. Gao, Confined nanobubbles shape the surface roughness structures of thin film composite polyamide desalination membranes, J. Membr. Sci., 582 (2019) 342-349.

[50] P. Lu, S. Liang, T. Zhou, T. Xue, X. Mei, Q. Wang, Layered double hydroxide nanoparticle modified forward osmosis membranes via polydopamine immobilization with significantly enhanced chlorine and fouling resistance, Desalination, 421 (2017) 99-109.

[51] X.-H. Ma, Z.-K. Yao, Z. Yang, H. Guo, Z.-L. Xu, C.Y. Tang, M. Elimelech, Nanofoaming of polyamide desalination membranes to tune permeability and selectivity, Environ. Sci. Technol. Lett., 5 (2018) 123-130.

[52] X. Song, J.W. Smith, J. Kim, N.J. Zaluzec, W. Chen, H. An, J.M. Dennison, D.G. Cahill, M.A. Kulzick, Q. Chen, Unraveling the morphology-function relationships of polyamide membranes using quantitative electron tomography, ACS Appl. Mater. Interfaces, 11 (2019) 8517-8526.

[53] A.K. Ghosh, E.M.V. Hoek, Impacts of support membrane structure and chemistry on polyamide–polysulfone interfacial composite membranes, J. Membr. Sci., 336 (2009) 140-148.

[54] X. Ma, Z. Yang, Z. Yao, H. Guo, Z. Xu, C.Y. Tang, Tuning roughness features of thin film composite polyamide membranes for simultaneously enhanced permeability, selectivity and anti-fouling performance, J. Colloid Interface Sci., 540 (2019) 382-388.

[55] L.E. Peng, Z. Yao, X. Liu, B. Deng, H. Guo, C.Y. Tang, Tailoring polyamide rejection layer with aqueous carbonate chemistry for enhanced membrane separation: Mechanistic Insights, chemistry-structure-property relationship, and environmental implications, Environ. Sci. Technol., 53 (2019) 9764-9770.

[56] M.R. Chowdhury, L. Huang, J.R. McCutcheon, Thin film composite membranes for forward osmosis supported by commercial nanofiber nonwovens, Ind. Eng. Chem. Res., 56 (2017) 1057-1063.

[57] G. Han, B. Zhao, F. Fu, T.-S. Chung, M. Weber, C. Staudt, C. Maletzko, High performance thin-film composite membranes with mesh-reinforced hydrophilic sulfonated polyphenylenesulfone (sPPSU) substrates for osmotically driven processes, J. Membr. Sci., 502 (2016) 84-93.

[58] J.T. Arena, S.S. Manickam, K.K. Reimund, P. Brodskiy, J.R. McCutcheon,

Characterization and performance relationships for a commercial thin film composite membrane in forward osmosis desalination and pressure retarded osmosis, Ind. Eng. Chem. Res., 54 (2015) 11393-11403.

[59] B. Khorshidi, T. Thundat, B.A. Fleck, M. Sadrzadeh, A novel approach toward fabrication of high performance thin film composite polyamide membranes, Sci. Rep., 6 (2016) 22069.

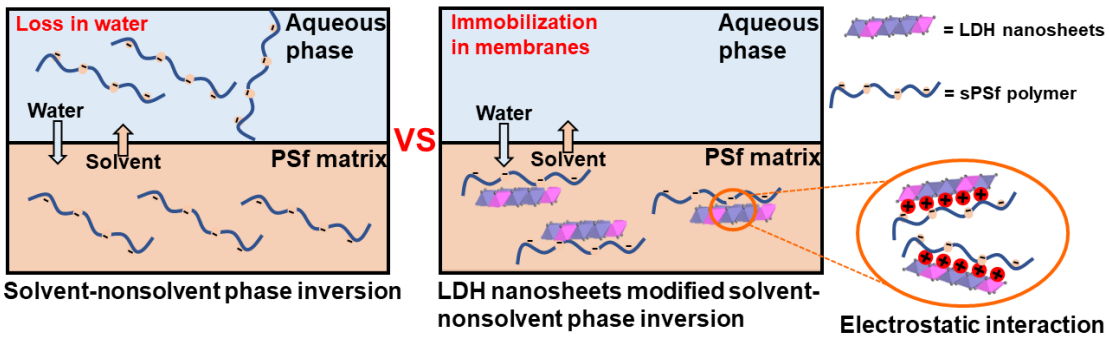

Figure 1. Comparison of the traditional solvent-nonsolvent phase inversion and the LDH nanosheets modified solvent-nonsolvent phase inversion.

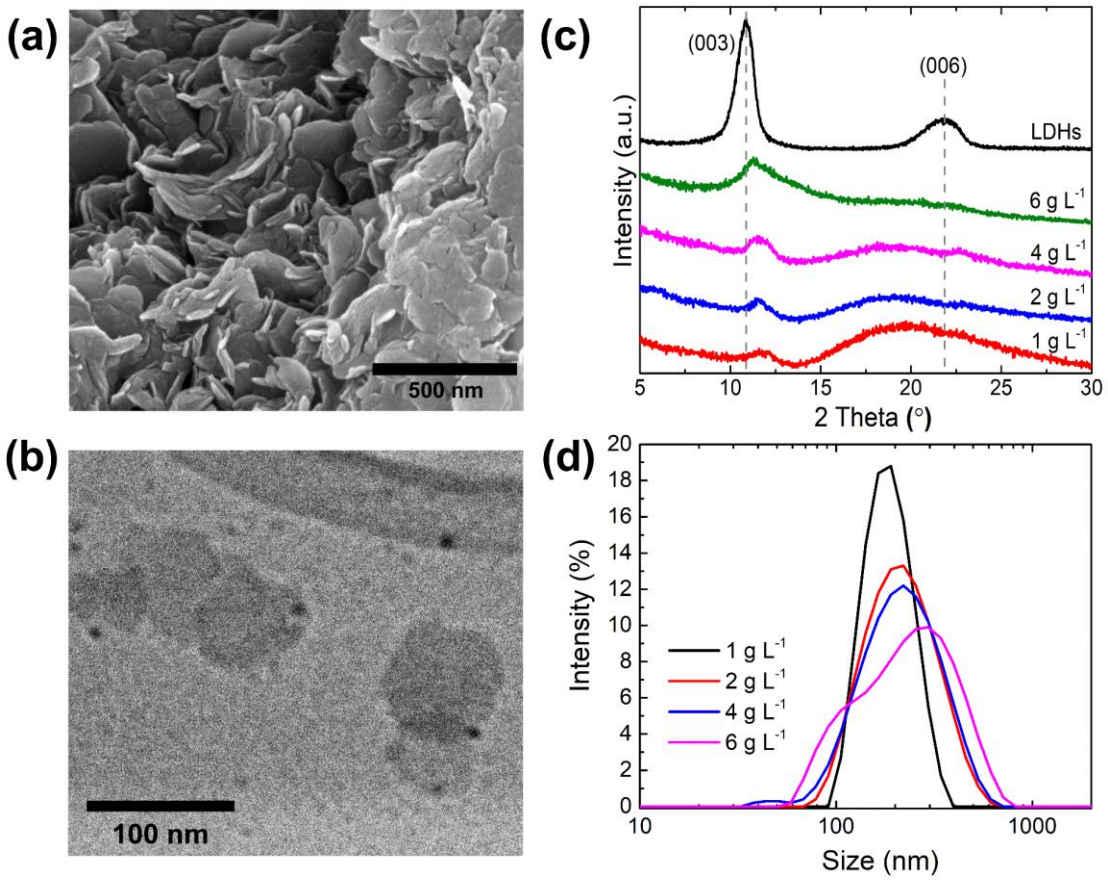

Figure 2. (a) SEM image of MgAl-NO_3 LDHs; (b) TEM image of exfoliated LDH nanosheets; (c) XRD patterns of MgAl-NO_3 LDH and exfoliated LDH nanosheets with different concentration; and (d) The particle size distribution of delaminated LDH dispersions with different concentration.

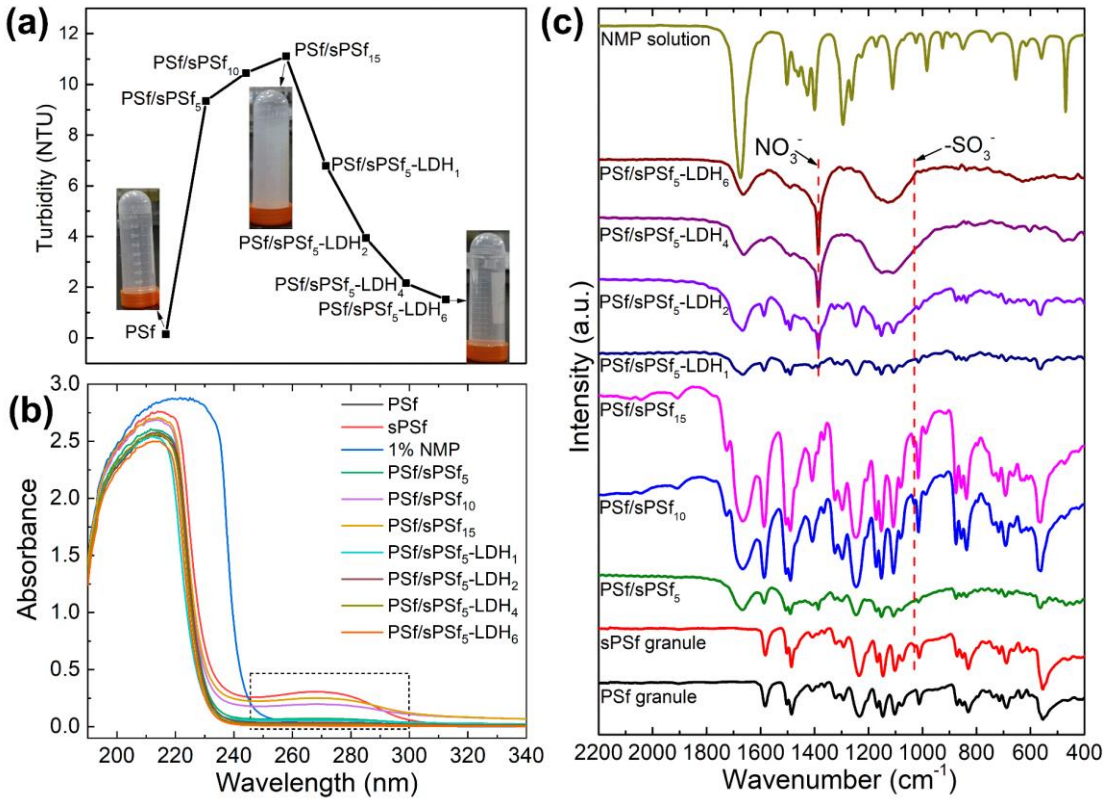

Figure 3. (a) The turbidity of coagulation baths; (b) UV–Vis spectra of coagulation baths and 1% NMP-water solution; and (c) ATR-FTIR spectra of NMP solution, PSf and sPSf granules, and the residues of coagulation baths after phase-inversion.

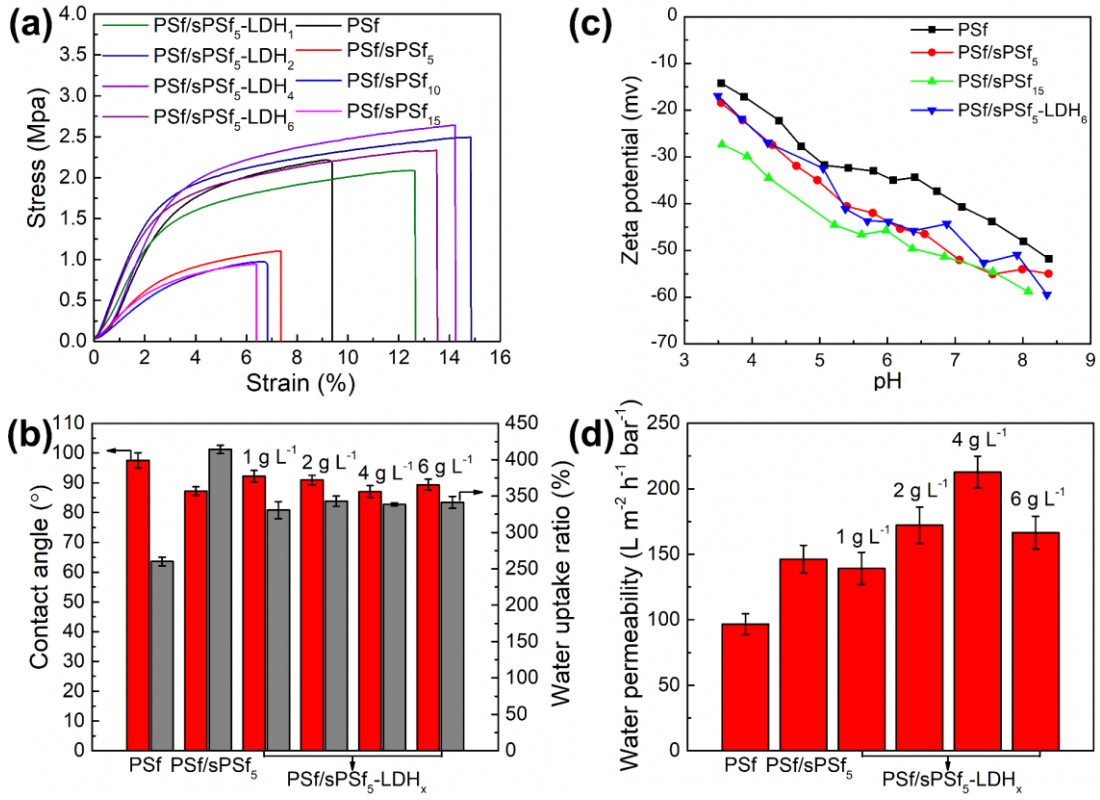

Figure 4. (a) Mechanical strength, (b) Water contact angle and water uptake ratio, (c) Surface zeta potential, and (d) Water permeability of the prepared substrates.

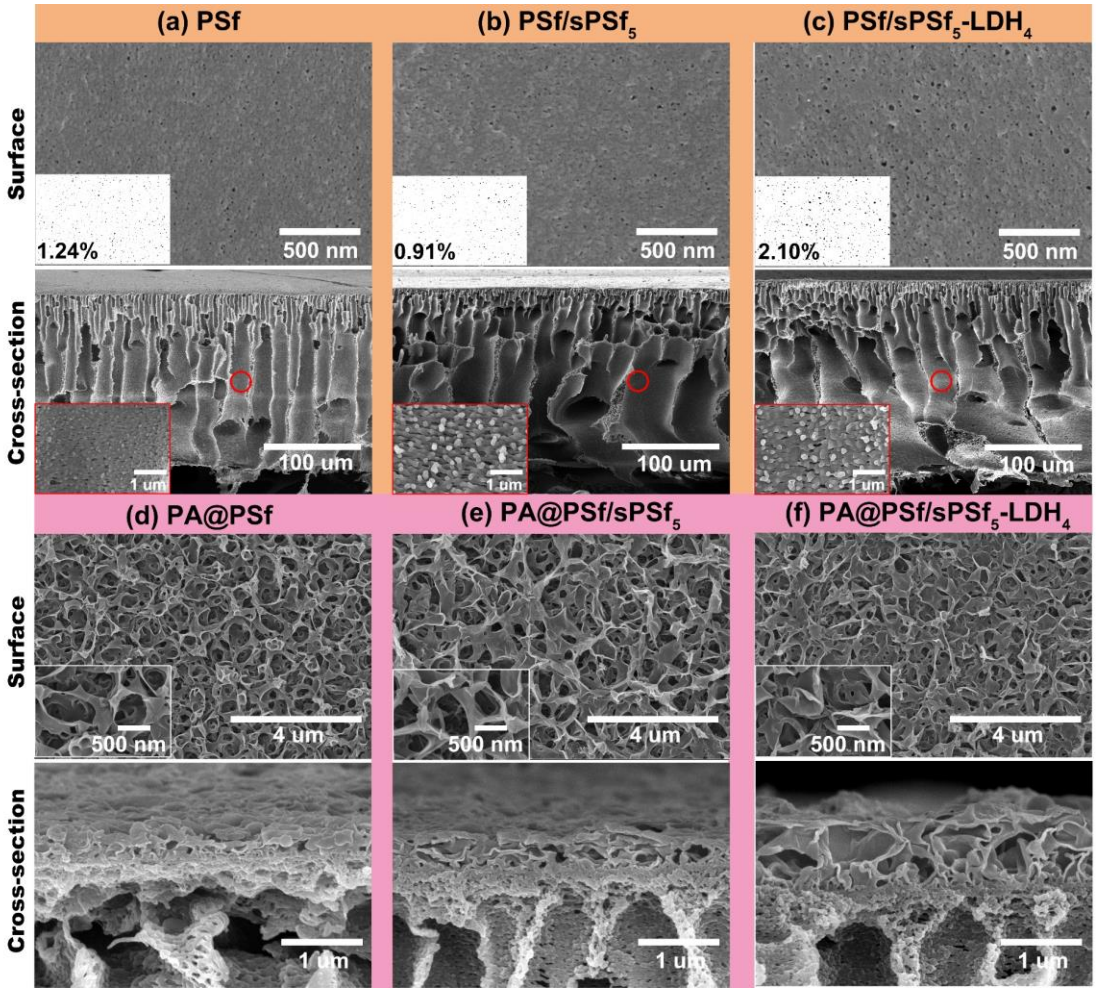

Figure 5. SEM images of the surface and cross–section of prepared substrates and PA-based TFC membranes. (a) PSf, (b) PSf/sPSf$_5$, and (c) PSf/sPSf$_5$-LDH$_4$ substrates; (d) PA@PSf, (e) PA@PSf/sPSf$_5$, and (f) PA@PSf/sPSf$_5$-LDH$_4$ membranes.

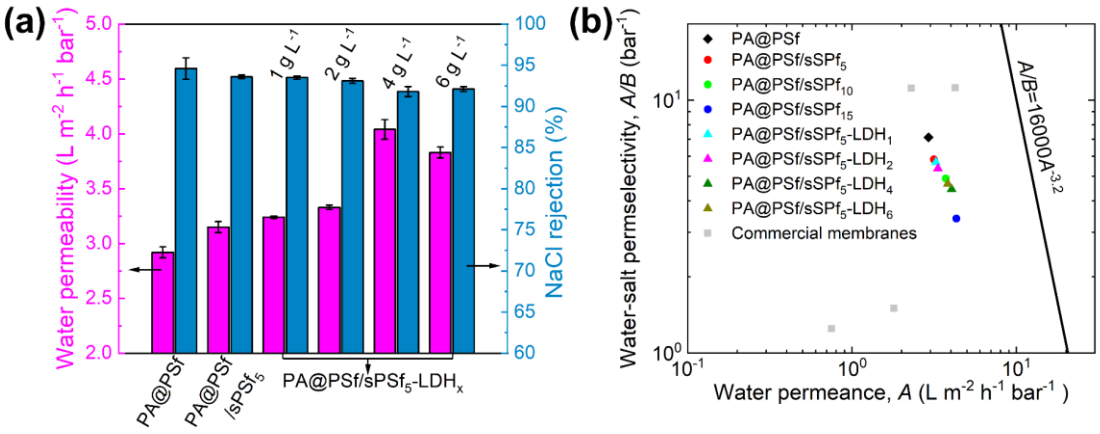

Figure 6. (a) Water permeability and NaCl rejection of prepared PA-based TFC membranes (ΔP =3 bar, DI-water and 10 mM NaCl as feed solutions for permeability and NaCl rejection of membrane, respectively); (b) Water permeability and water-NaCl permselectivity of prepared PA-based TFC membranes and commercial membranes [6, 56-58] relative to the "upper-bound".

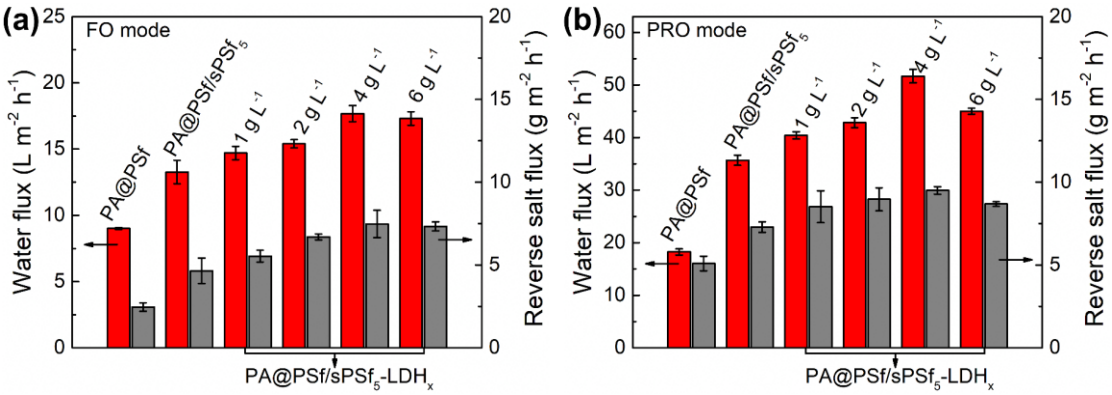

Figure 7. Water and reverse salt fluxes of prepared PA-based TFC membranes (a) FO mode, (b) PRO mode (1 M NaCl as DS, DI-water as FS, and cross–flow rate is 0.45 L min^{-1}).

Table 1. Composition of casting solutions.

Membranes	PSf (wt%)	sPSf (wt%)	NMP (wt%)	LDH nanosheets concentration (g L^{-1})
PSf	12.0	-	88.0	-
PSf/sPSf$_5$[a]	11.4	0.6	88.0	-
PSf/sPSf$_{10}$	10.8	1.2	88.0	-
PSf/sPSf$_{15}$	10.2	1.8	88.0	-
PSf/sPSf$_5$-LDH$_1$[b]	11.4	0.6	88.0	1.0
PSf/sPSf$_5$-LDH$_2$	11.4	0.6	88.0	2.0
PSf/sPSf$_5$-LDH$_4$	11.4	0.6	88.0	4.0
PSf/sPSf$_5$-LDH$_6$	11.4	0.6	88.0	6.0

[a]The subscript corresponds to the content of sPSf in the total mass of polymers.

[b]The subscript corresponds to the concentration of delaminated LDH dispersions.

Immobilization of sulfonated polysulfone via 2D LDH nanosheets during phase-inversion: A novel strategy towards greener membrane synthesis and enhanced desalination performance

Peng Lu[1,2], Yi Wang[3]*, Ling Wang[1,2], Yayu Wei[1,2], Wenjun Li[1,2], Yanshuo Li[1,2]*, Chuyang Y. Tang[4]*

[1]School of Materials Science and Chemical Engineering, Ningbo University, Ningbo, 315211, P. R. China

[2]State Key Laboratory Base of Novel Functional Materials and Preparation Science, School of Materials Science & Chemical Engineering, Ningbo University, Ningbo, 315211, P. R. China

[3]State Key Lab of NBC for Protect Civilian, Beijing, 102205, P. R. China

[4]Department of Civil Engineering, the University of Hong Kong, Pokfulam Road, 999077 Hong Kong, S.A.R., P. R. China

We declare the submitted work is original and has not been published nor is considered for publication elsewhere. We declare no competing financial interests.

Immobilization of sulfonated polysulfone via 2D LDH nanosheets during phase-inversion: A novel strategy towards greener membrane synthesis and enhanced desalination performance

Peng Lu[1,2], Yi Wang[3]*, Ling Wang[1,2], Yayu Wei[1,2], Wenjun Li[1,2], Yanshuo Li[1,2]*, Chuyang Y. Tang[4]*

[1]School of Materials Science and Chemical Engineering, Ningbo University, Ningbo, 315211, P. R. China

[2]State Key Laboratory Base of Novel Functional Materials and Preparation Science, School of Materials Science & Chemical Engineering, Ningbo University, Ningbo, 315211, P. R. China

[3]State Key Lab of NBC for Protect Civilian, Beijing, 102205, P. R. China

[4]Department of Civil Engineering, the University of Hong Kong, Pokfulam Road, 999077 Hong Kong, S.A.R., P. R. China

We declare the submitted work is original and has not been published nor is considered for publication elsewhere. We declare no competing financial interests.